STUDY OF ADSORPTION OF BIOLOGICAL AND NANOPARTICLE SOLUTIONS AT THE SOLID-LIQUID INTERFACE

by

DANIEL WAYNE FROST

B.S., University of Arkansas, 2005

A REPORT

submitted in partial fulfillment of the requirements for the degree

MASTER OF SCIENCE

Department of Physics
College of Arts and Sciences

KANSAS STATE UNIVERSITY
Manhattan, Kansas

2007

Approved by:

Major Professor
Bruce Law

Abstract

With advances in micromechanical machining and nanotechnology, the sample volume needed for biological research and other analysis decreases. With small volume, sample-surface interactions including adsorption must be considered. These adsorption effects can be observed by analyzing light reflected from the solid-liquid interface, and the contact angle of a solution on the surface. Presented is the design and construction of an ellipsometer, a device used to analyze light reflected off of a solid-liquid interface to find interfacial properties, including thickness of a thin film formed by adsorption. The taq enzyme is shown to have a large change in contact angle from seventy degrees to about ten degrees over a short (ten minute) time period when placed on an SU-8 substrate, indicating a change in energy at the interface and a large amount of adsorption. Silane substrates are found to produce similar results. Ellipticity of a colloidal gold nanoparticle solution on a glass substrate is also observed, whose results are difficult to interpret due to bulk shifts in the sample. With the ellipsometer running correctly, it can be used for a number of experiments, including spectroscopic ellipsometry and Brewster angle microscopy, with some modifications.

Table of Contents

List of Figures

Acknowledgements

I would like to thank my major professor Dr. Bruce Law for the massive amount of time he contributed in the form of guidance and assistance in this project, and for lending words of encouragement when the going got tough (which it did quite often). I would also like to thank Dr. Chris Sorensen, who supported me not only as the NIRT chairperson, but also as a teacher. I would also like to thank the other members of the Law liquid surfaces group, notably Sean McBride, who helped greatly in the construction of the ellipsometry apparatus.

Dedication

For my family, who always found time to support me during my college career.

CHAPTER 1 - Introduction

One of the biggest advances in genetic analysis in recent years has been the development of machining of micro-electrical and micromechanical systems, and the development of nanoparticles and nanotechnology. These have resulted in a reduction of size and complexity of analysis systems to, in some cases, the size of a credit card (Prakash *et al.,* 2005). With the reduction of analysis volumes, however, the interaction between a sample and the surface of the microfluidic device becomes more important. Surfaces must be chosen carefully to oppose interference at the sample-surface interface, or encourage it if that is the desired result. The primary focus of this work was the development of a device to analyze interactions at the interface, and to test both biological and nanoparticle solutions at a various solid-liquid interfaces.

Figure 1.1 Example of a Lab-on-a-Chip Used in Micro Fluidic Analysis

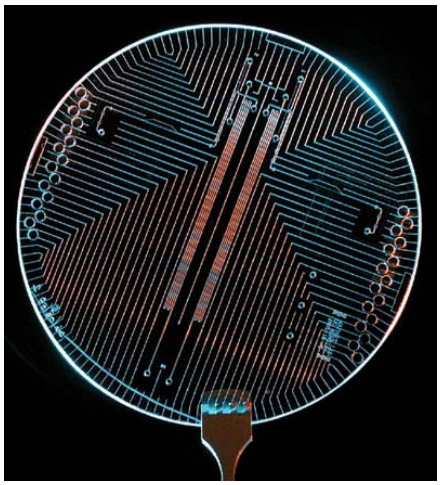

From Nature (Marris, 2006) –This entire wafer is 100mm wide.

Amongst the interactions to be concerned with, and the primary focus of the experiment, is adsorption, whereby a solute dissolved in a solution is extracted by the solid surface the solution is applied to, forming a thin film on the surface and diluting the solution. This reduction in concentration can affect the process one is trying to observe, including genetic processes (Prakash *et al.,* 2005). The change in surface structure can also affect the slip (the velocity of the

solution at the interface itself) of the surface. In some cases, this extraction is the goal of the process, such as in water and air purification.

The surface structure also affects surface energy at the interface, which in turn affects how well the solution wets the surface (how well the solution is attracted with the substrate), and the polarization of light reflected off of the interface. Both of these properties can be measured to indicate the thickness of the thin film of solute that forms on the surface, and thus the amount and speed of the adsorption occurring at the interface. After design and construction of the measurement apparatus, this initial work focused primarily on two types of solutions.

Experimental Solutions

The first of the experiments conducted focused on adsorption of a biological solution of diluted taq enzyme on an SU-8 photoresist substrate. This biological sample was chosen because, when applied to some substrates, there appears to be a large amount of adsorption at the solution-substrate interface. Previous research on the enzyme solution by A. Ranjit Prakash at the University of Calgary had shown a contact angle change (a measure of wetability) of approximately 60 degrees over a ten minute period in this setup. One of the ultimate goals of this research is to understand in more detail what is occurring at the surface as this adsorption occurs.

Figure 1.2 Experimental Contact Angle vs. Time for Taq Enzyme on an SU-8 Substrate, as Measured by A. Ranjit Prakash at the University of Calgary (Unpublished)

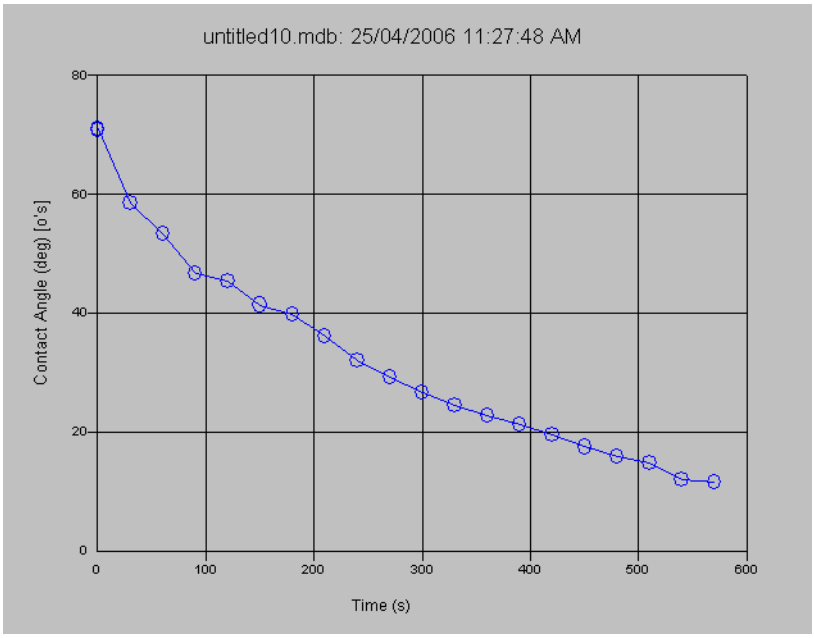

The taq polymerase is an enzyme vital to the polymerase chain reaction, a process that allows one to extract a section of DNA and amplify it by reproduction. Since it was introduced in 1985, it has been used in many of biological applications (Auroux *et al.,* 2004). In this process, the DNA is denatured into its separate strands by heating to 95 degrees Celsius. The temperature is reduced to around 60 degrees C, and primers attach themselves to these single strands in the portion to be reproduced. The temperature is raised to 72 degrees Celsius, and the taq synthesizes new DNA based on the strand template.

SU-8 is an epoxy-based photoresist used in the construction of microscopic structures and components. It is unique among photoresists as it can be spin coated to a thickness of up to 300 μm and has a high aspect ratio (ratio of the smallest possible width of a gap with the gap's thickness) of 10 to 12. In summary, the structure creation process consists of spin coating the SU-8 onto a Si wafer or other substrate. The coat is softbaked, and the areas that want to be kept (the structures themselves) are exposed to UV light. The exposure results in a cross-linking of the exposed layer's molecular chains, making those areas highly resistant to solvents. After a second bake, the surface is dipped into a developer, which strips the unexposed portions of the SU-8 layer, leaving the desired structure. SU-8 is one of the more ideal photoresists used to produce microelectromechanical systems (MEMS) (Lorentz *et al.,* 1997).

Figure 1.3 Example of a Structure Created using the SU-8 Photoresist

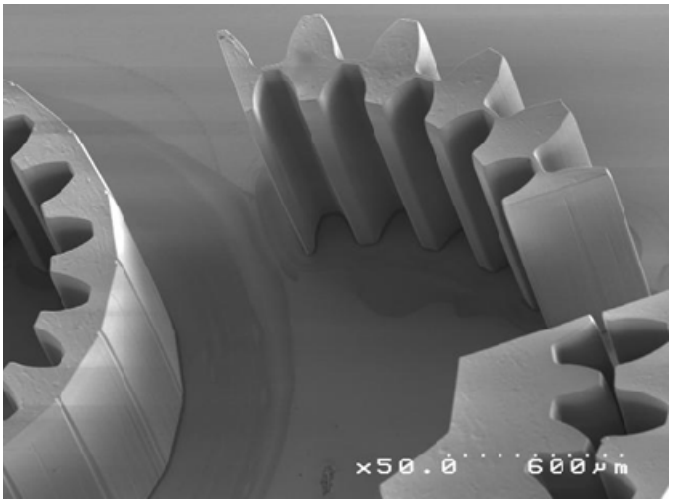

From (Chollet, 2007)

The second part of the experiment, conducted with the ellipsometer, concerned adsorption of a gold nanoparticle (NP) solution on glass, particularly, the change in surface

properties during the assembly of a thin nanoparticle film. The colloidal gold nanoparticles used in this experiment were constructed by the KSU NIRT (Nanoscale Interdisciplinary Research Team) via a digestive ripening method, utilizing dodecanethiol as discussed in previous literature (Prasad *et al.*, 2002). In brief, AuCl3 is added to a solution of dodecyldimethylammonium bromide in toluene, and NaBH4 solution is slowly added to form the colloid. Dodecanethiol is added, and the byproducts of the reaction removed. The particles are dried, and toluene is added.

CHAPTER 2 - Theory

In this chapter, the theory behind ellipsometry is discussed, including the process by which interface thickness is calculated from interface energy and contact angle.

Ellipsometry

The surface energy and other properties of an interface between two media affect the polarization of light reflected off of it. A change in this energy due to adsorption and formation of a thin film changes this polarization. By reflecting polarized light off of the interface, and measuring the resulting polarization and change in intensity, properties of the interface can be observed. This is the basis behind ellipsometry.

When discussing polarization in regards to ellipsometry, the polarizations of concern are the P orientation, which represents the electric field component parallel to the light's plane of incidence (and perpendicular to the interface in question), and the S orientation, which represents the electric field component perpendicular to the plane of incidence. The electric field vector of an unpolarized, monochromatic light wave will have components in both directions. Over time, this vector will travel through the P-S plane in an ellipse, whose shape is dependent on the magnitude of the P and S components and the phase difference between both components. If there is no phase difference between the components, the resulting electric field vector travels in a line, and the light is linearly polarized. If there is a quarter wavelength phase difference between the two components, and both components have equal amplitude, the vector travels in a circle, and the light is circularly polarized, otherwise, the field vector travels in an ellipse (Hecht, 2002).

Figure 2.1 Example of a Right-Handed (Clockwise) Polarization Ellipse

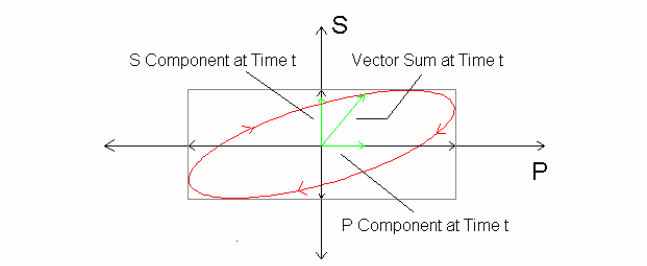

The complex ratio of the amplitudes in each polarization (the farthest extent of the box in Figure 2.1 above) is known as the ellipticity.

$$r_p / r_s = \rho\left(e^{i\Delta}\right) \quad \ldots(2.1)$$

In this equation, r_p and r_s represent the amplitudes in the P and S polarizations, ρ is the ellipticity, and Δ is the phase shift between the P and S components. When light is incident on the interface at the Brewster angle (at which only S polarized light is reflected), the real part vanishes, and the remaining imaginary part is known as the coefficient of ellipticity ($\bar{\rho}$).

Drude found the relation between the coefficient of ellipticity and the dielectric constant of the media composing the interface, and a thin transition region between the media (the thickness of which << λ). Drude's equation represents a correction to the familiar Fresnel equations, accounting for the transition region between the two media,

$$\bar{\rho} = \frac{\pi}{\lambda}\frac{\sqrt{\varepsilon_1 + \varepsilon_2}}{\varepsilon_1 - \varepsilon_2}\eta \quad \ldots(2.2)$$

$$\eta = \int \frac{(\varepsilon - \varepsilon_1)(\varepsilon - \varepsilon_2)}{\varepsilon} dz \quad \ldots(2.3)$$

where λ represents the wavelength of the incident light, and $\varepsilon_1, \varepsilon_2, \varepsilon$ represent the first medium's dielectric constant, second medium's dielectric constant, and the intermediate dielectric constant as a function of z (through the profile of the media, see Figure 2.2), respectively (Beaglehole, 1980).

<u>Figure 2.2</u> Dielectric Profiles Through Two Types of Interfaces

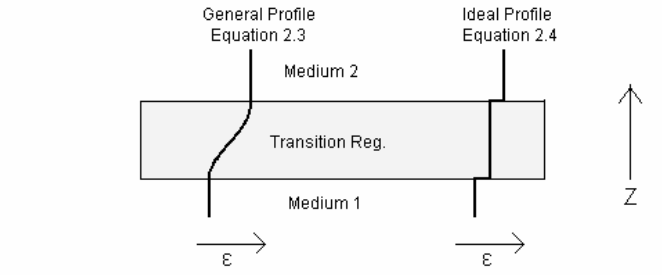

For the ideal situation of molecularly smooth surfaces on the media, and a constant dielectric constant throughout the transition region, which represents the adsorption layer between our substrate and experimental solution, equation 2.3 can be simplified as

$$\eta = \frac{(\varepsilon - \varepsilon_1)(\varepsilon - \varepsilon_2)}{\varepsilon} t \quad \ldots(2.4)$$

where t is the thickness of the transition region. In this ideal situation, the thickness of the film can easily be found (Beaglehole, 1980). Additional layers in this system (multiple interfaces) complicate the calculations greatly, thus the experimental system was designed as simple as possible (see chapter 3). By observing changes in $\overline{\rho}$, changes in the thickness of the adsorption layer can be observed over time.

Contact Angle

When a liquid is brought into contact with a solid, the liquid's spread onto the solid surface is dependent on the surface energy of the solid. The resulting shape of the liquid drop is dependent on forces at the three interfaces. For a sample solution drop on a solid substrate sitting in air, these interfaces are located at the solid-vapor boundary, the liquid-vapor boundary, and the liquid-solid boundary, where adsorption occurs and the experiment is concerned with. The forces are related by Young's equation

$$\sigma_{SV} = \sigma_{SL} + \sigma_{LV}(\cos\theta) \quad \ldots(2.5)$$

where $\sigma_{SV}, \sigma_{SL}, \sigma_{LV}$ are the energy per unit area at the solid-vapor (the solution's surface tension), solid-liquid, and liquid-vapor interfaces, respectively. θ is the contact angle of the liquid on the solid, a measure of how much the liquid 'wets' the surface (how far the drop spreads out on the surface).

<u>Figure 2.3</u> Diagram of the Forces that Determine Contact Angle

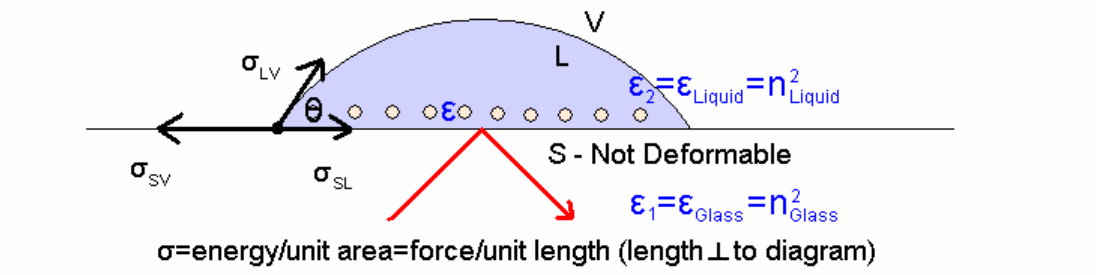

When the surface energy at the solid-liquid interface is high or the solution's surface tension is low, the contact angle is small and the drop spreads out over the surface. In this case, the surface is said to be wetable, and is called hydrophilic. When the surface energy is low, the

solution ‘balls up’ on the surface. This non-wetable surface is hydrophobic. Between these, at around 90 degrees, the surface is an intermediate.

<u>Figure 2.4</u> Examples of a Slightly Hydrophobic Surface (L) and a Hydrophilic Surface (R)

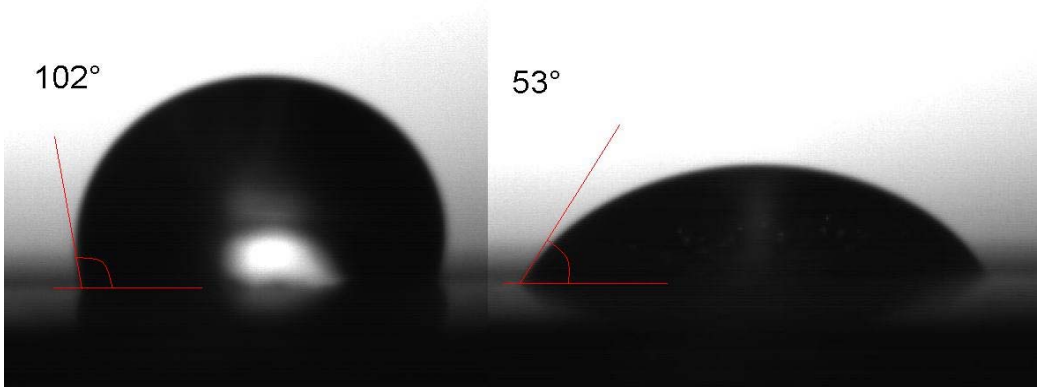

As adsorption occurs at the liquid-solid interface, formation of the transition layer results in a change of surface energy. Observation of the contact angle is another way to observe the adsorption process as it occurs.

CHAPTER 3 - Apparatus and Methods

The Inverted Ellipsometer

For the purposes of the liquid-solid interface experiments, an ellipsometer was designed and constructed such that the incident laser light strikes the underside of a glass sample slide, on which a substrate has been applied, and on which the sample drop is applied. This was achieved by disassembling an existing top-incident ellipsometer not in use and constructing new hardware such that the 'arms' hang down. The first part of this section briefly describes the design process, while the second details alignment and calibration.

Design

The ellipsometer is based on a design by Dr. Bruce Law (Law, 1984), which in turn was based on a design by Beaglehole (Beaglehole, 1980). By imposing a high frequency AC signal on the incident laser light, an AC lock-in can be used to detect the resulting signal, eliminating much of the DC noise, while a gain control feedback system keeps the DC portion of the signal constant, simplifying the calculations in below. Computer control of the various components (the lock-ins, the ellipsometer arms) adds some automation to the experiment.

The lock-in detection system used in this experiment is modified from Law's. Law used an oscillating analyzer to measure signals from both +45 degree and -45 degree (to the P polarization) orientations using the same photomultiplier detection device. This imposed an additional phase to the signal in addition to the ones present, requiring a third lock-in in addition to the lock-ins measuring the ω_0 and $2\omega_0$ components of the signal. The lock-in system used in this experiment measures signals from both orientations simultaneously. This is accomplished by sending the reflected signal through a Wollaston prism, aligned to split the reflected flux into its orthogonal components at ±45 degrees.

Each signal is sent to its own detector which is integrated into separate lock-in and feedback systems. Two lock-ins were utilized, with each measuring both the ω_0 and $2\omega_0$ signals for each orientation. Switching between frequencies does limit the observation rate; however, as one data point can be taken every 21 seconds. Addition of two additional lock-ins (whereby each

measures either of the orientations at only one of the frequencies) would speed data collection, but that option was not integrated due to cost concerns and the fact that the present collection rate was found to be adequate.

The apparatus first consists of a He-Ne laser (1 in Figure 3.1 below) with a wavelength λ=632.8nm and power output of 5mW (Melles-Griot 05-LHR-141). The original Law design included neutral density filters following the laser, but the addition of two additional ground glass diffusers in the current analyzer made the signal too weak to be analyzed with the filters. The light is then sent through a polarizer (2) aligned at +45 degrees to the P orientation and modulated at ~ 50 kHz by a birefringence modulator (3). The laser light travels through one of the legs of a right prism (Edmund Optics Fused Silica) (4), which has been mounted on a three axis translation system in a prism holder designed by the author, and custom-built by Sean McBride (5), and aligned such that its hypotenuse lies flat. A glass slide coated with the substrate under analysis on which the sample drop is applied, or a sample chamber which contains the solution under analysis, is affixed onto the prism using index matching fluid (Cargille Labs #19571 n=1.4587). This eliminates any air filled space between the prism and glass which would add another interface and complicate interface thickness calculations. Even with the matching fluid, a second reflection (E_1 in Figure 3.1) occurs when a substrate is present, due to the glass-substrate interface. Theoretical work is being conducted of the effect this substrate may have on our results.

Figure 3.1 The Inverted Ellipsometer and Sample Surface

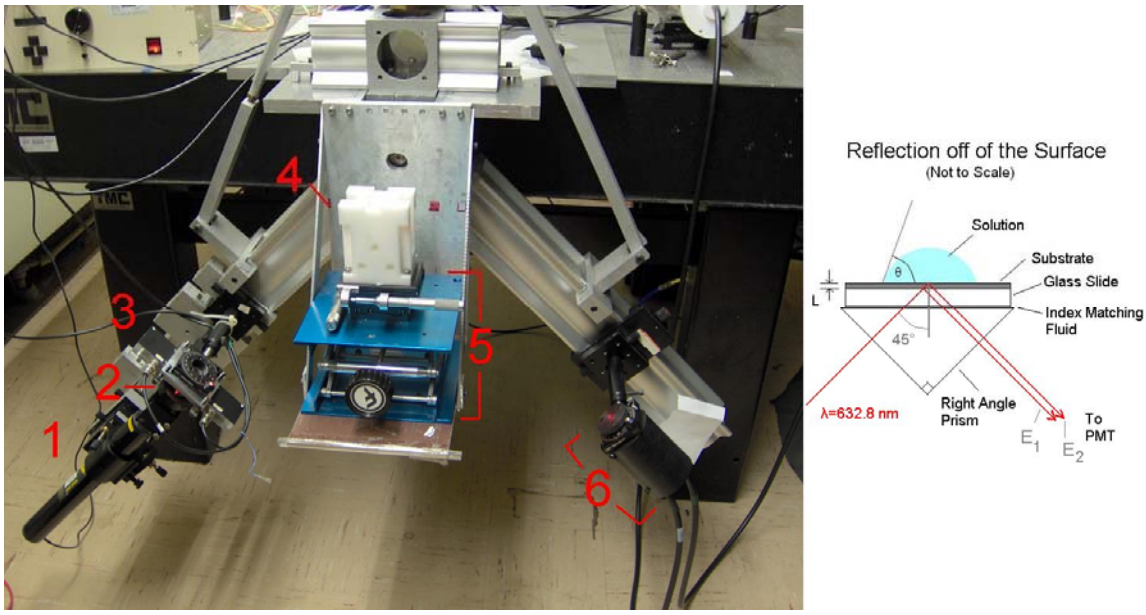

After reflection off of the substrate-sample interface, light travels into the analyzer (6). In the analyzer, the light first passes through a He-Ne filter. It then passes through a Wollaston prism (ThorLabs WP10, 20 degree angular deviation), aligned such that its outgoing beams are linearly polarized at ±45 degrees to the P orientation. Measurement at both of these orientations reduces errors due to small movements and imperfections in the system. Each beam passes through two 1.6 mm ground glass diffusers, separated by one inch. These expand the beam, allowing them to completely fill the following fiber optic cables, which minimizes errors caused by small shifts in the position of the incident beam on the cable. The light is carried by the fiber optics to separate photomultipliers, where each beam hits an additional scatter glass before acquisition by the detector.

Construction

The birefringence modulator used in this experiment had been pre-constructed for an earlier experiment, and its construction will be briefly discussed here. The modulator consists of an optical glass rod, with two piezoelectric quartz crystals cemented on both ends with a quick setting adhesive. Two sides of the quartz crystals are coated with a thin layer of highly conductive Silver Print, and an additional amount of print is used to set and attach each rod between a pair of thin wires.

<u>Figure 3.2</u> Front and Side Views of the Birefringence Modulator and the Longitudinal Strain Relative to the Crystals

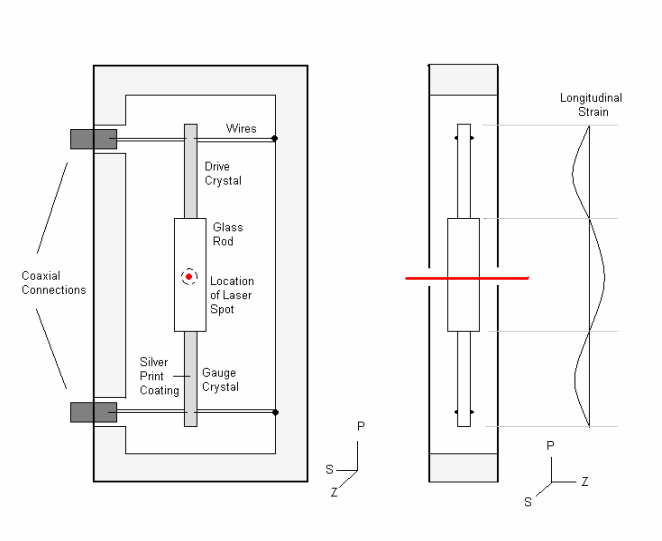

When an AC voltage is applied to the drive crystal, it creates a longitudinal strain standing wave throughout the modulator (see Figure 3.1). The strain in the central glass rod imparts a phase shift δ between the P direction, whose axis is the same as the strain axis of the glass rod, and the S direction orthogonal to it. This strain also results in a voltage at the gauge crystal. This reference voltage is kept constant by feedback to the drive oscillator, which maintains this reference by adjusting the drive voltage.

The analyzer, containing the Wollaston splitting prism and glass diffusers, was built from scratch with machining help from Sean McBride. The prism itself is fixed inside a rotation mount using hardened paraffin wax. Attached to the front of the stage is a custom-made cap containing the He-Ne filter. The analyzer itself is attached to the other side of the rotation mount. Two one-quarter inch diameter shafts were drilled through a Delrin rod at an angle of ten degrees from the center of the rod. Larger shafts (3/4 inch diameter on the exit side, 1/2 inch on at the entrance) were partially drilled into these smaller shafts to accommodate the glass diffusers, which are secured with double-sided tape. Plugs were custom made to fit our fiber optics with the analyzer, and the entrance side was machined until the Wollaston prism split the incoming laser down the center of each shaft.

<u>Figure 3.3</u> Diagrams and Image of the Wollaston Analyzer

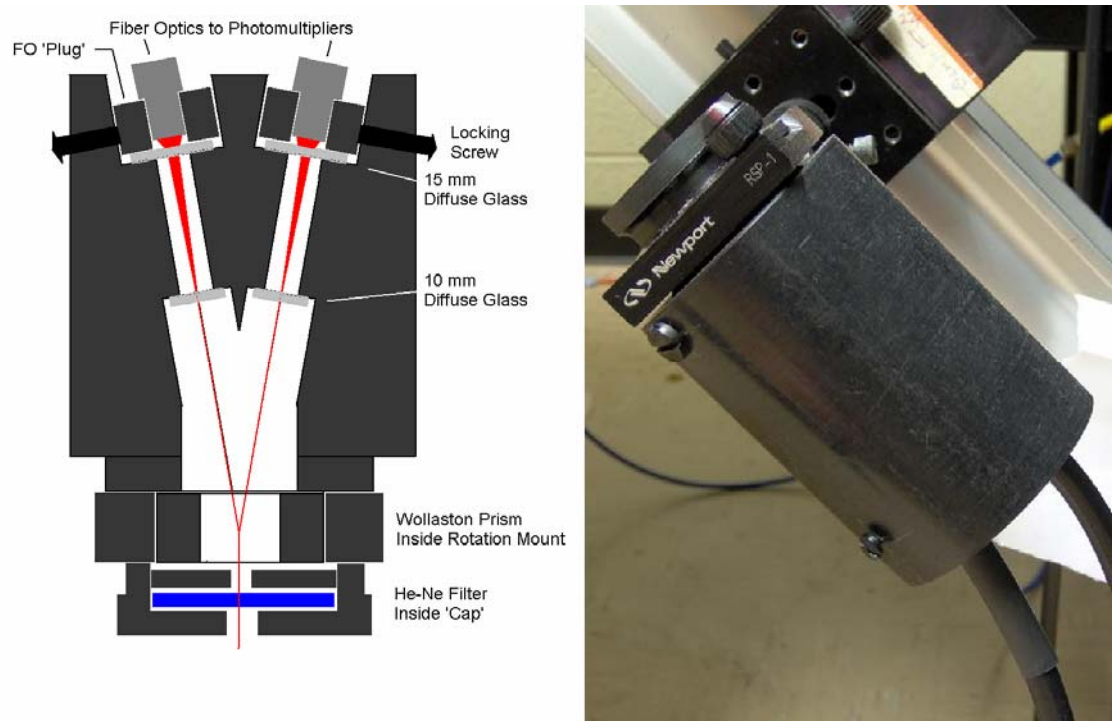

A gain controller was also built to accommodate the second photomultiplier and feedback system. The gain controller feedback system adjusts the output of the photomultiplier's programmable high voltage power supply (Bertan 205B-03R) such that the resulting amplified signal's DC component is kept constant, while the ω_0 and $2\omega_0$ AC signals are unaffected. Once calibrated, these DC signals fall out of the calculation, and the measured signal becomes independent of system parameters, such as the type of photomultiplier.

High Speed Camera and Microscope System

A high speed camera and microscope (Artray ARTCAM 130 MIBW with Navitar 12x Zoom 12mm FF lens) and drop shape analysis software (First Ten Angstroms FTA32) allow for simultaneous experimentation and video capture of the sample drop. The sample is back lit using an adjustable light source, and the resulting video can be saved and analyzed frame-by-frame for drop contact angle, base width and size, drop volume, surface tension, and other parameters. Examples of images taken by the camera system can be found in chapter 4.

Description of Light in the Ellipsometer

The following is a brief discussion of waveforms of the laser light as it travels through the ellipsometer. A detailed analysis can be found in Appendix A and in previous literature (Law, 1984).

The initial laser light is polarized at +45 degrees to the P orientation. The birefringence modulator imposes an additional phase shift δ in the P orientation alone. The complex electric field becomes

$$\tilde{\tilde{E}} = \frac{E_0}{\sqrt{2}}\left(\hat{\tilde{s}} + e^{i\delta}\hat{\tilde{p}}\right) \quad \ldots(3.1)$$

reflection off of the interface results in a phase shift δ_i and change in amplitude r_i in both orientations, resulting in

$$\tilde{\tilde{E}} = \frac{E_0}{\sqrt{2}}\left(\left|r_s\right|e^{i\delta_s}\hat{\tilde{s}} + \left|r_p\right|e^{i\left(\delta_p+\delta\right)}\hat{\tilde{p}}\right) \quad \ldots(3.2)$$

and an intensity (the complex square of the field) of

$$I = \left|\tilde{E}\right|^2 = \left(\frac{E_0}{2}\right)^2 \left(\left|r_s\right| e^{i\delta_s} \hat{\tilde{s}} \pm \left|r_p\right| e^{i(\delta_p+\delta)} \hat{\tilde{p}}\right)^2 \quad \ldots(3.3)$$

where the ± is needed because the intensity is taken at both +45 degrees and -45 degrees to the P direction. After some simplification (see Appendix A)

$$I = \frac{I_0}{4}\left(r_s{}^2 + r_p{}^2\right)\left(1 \pm a\cos(\Delta + \delta)\right) \quad \ldots(3.4)$$

where $I_0 = E_0{}^2$, and

$$\Delta = \delta_p - \delta_s$$

$$a = \frac{2r_s r_p}{r_s{}^2 + r_p{}^2} = \frac{2r_s{}^2\left(r_p / r_s\right)}{r_s{}^2\left(1 + \left(r_p{}^2 / r_s{}^2\right)\right)} = \frac{2\rho}{1+\rho^2}, \rho = \frac{r_p}{r_s} \quad \ldots(3.5)$$

The phase shift created by the modulator varies sinusoidal at angular frequency ω_0, thus

$$\sin(\delta) = \sin(\delta_0 \sin \omega_0 t), \cos(\delta) = \cos(\delta_0 \sin \omega_0 t) \quad \ldots(3.6)$$

where δ_0 is proportional to the strain amplitude. This term can be expanded into a series of Bessel functions, and the resulting intensity (to the first three Bessel terms) is

$$I = \frac{I_0}{4}\left(r_s{}^2 + r_p{}^2\right)\left(1 \pm a\left[\cos\Delta J_0(\delta_0) - \sin\Delta 2J_1(\delta_0)\sin(\omega_0 t) + \cos\Delta 2J_2(\delta_0)\cos^2(\omega_0 t)\right]\right)$$

$\ldots(3.7)$

The second and third terms in brackets represent the ω_0 and $2\omega_0$ AC components of the signal, and the δ_0 dependence is removed from the first term by finding δ_0 such that $J_0(\delta_0)=0$. This is easily done during the calibration, and the resulting first term

$$I_{DC} = \frac{I_0}{4}\left(r_s{}^2 + r_p{}^2\right) \quad \ldots(3.8)$$

represents the DC component of the signal, kept fixed within 0.1% by the gain control feedback system.

Alignment and Calibration

The laser, polarizer, and modulator are mounted on the left ellipsometer arm, and the analyzer is mounted on the right arm (Figure 3.1 above). The arms are built to be moved

together, using a stepping motor and computer controlled motor controller. To align, the arms are set to the horizontal and the laser and analyzer are added, and alignment points are placed along the arms. The points are set to the same length, and the laser adjusted such that it passes through the tip of each point. The analyzer is adjusted so that the laser enters the center of the entrance pupil and reflected light is sent back to the center of the laser. The points are removed and the position of the analyzer is fine tuned until equal intensities are recorded at each of the exits.

The P and S orientations are found using the Brewster angle of the air-glass interface (the prism in the sample holder is used for this because of its well defined index of refraction n=1.458). The polarizer is added and adjusted so that reflected light passes back to the laser, and the arms are set at the air-glass Brewster angle. The polarizer is adjusted until a minimum intensity is recorded after reflection (P orientation). The arms are straightened again, and with the incoming light P polarized, S and P can be found on the analyzer by rotating it until a minimum output is recorded in one of the exits. The modulator is added and aligned to zero out the w_0 and $2w_0$ signals, and, after rotating the analyzer 45 degrees, its amplitude is adjusted so that equal DC components are recorded at each orientation (± 45 degrees), thus setting $J_0(\delta_0)=0$. This is done by observing the DC signal at one of the analyzer exits as the analyzer is being rotated between the two orientations. Only one exit is used, so any minor discrepancies between the two exits do not affect this calibration.

The calibration values consist of a phase shift, which allows the modulator's reference signal and the measured signal to be in sync for the lock-in technique, and a reference maximum signal to compare the observed signal with. These values are found first by adding a quarter wave plate (QWP), with the fast axis aligned with the P orientation, to the straightened arms and no sample. The QWP imparts a quarter wavelength difference between the S and P orientations, thus $\Delta=\pi/2$ and $\cos\Delta=0$ in equation 3.7 above, and with no sample $\rho=1$, thus only the second term in equation 3.7 is non-zero, and

$$I_{AC}(\omega_0)_{+45} \propto \left(\pm -2J_1(\delta_0)_{+45}\right) = I(\omega_0)_{cal(+45)} \quad \ldots(3.9a)$$

$$I_{AC}(\omega_0)_{-45} \propto \left(\pm -2J_1(\delta_0)_{-45}\right) = I(\omega_0)_{cal(-45)} \quad \ldots(3.9b)$$

The reference phase shift is set at the lock-in such that this signal is a minimum, and offset 90 degrees. The resulting phase shift and maximum value for I_{AC} represent the calibration values for this frequency at this orientation. A calibration value and phase is found for each polarization

orientation with the analyzer fixed in place, as the signals are measured simultaneously from each of the analyzer exits. The measurement from both exits removes the effect of any small discrepancies between the exits when the signal-calibration ratio is taken to find rho. The QWP is removed, and as a result $\Delta=0$ and $\sin\Delta=0$, thus only the third term in equation 3.7 remains and produces the ω_0 calibration values and phases

$$I_{AC}(2\omega_0)_{+45} \propto \left(\pm 2J_2(\delta_0)_{+45}\right) = I(2\omega_0)_{cal(+45)} \quad \ldots(3.10a)$$

$$I_{AC}(2\omega_0)_{-45} \propto \left(\pm 2J_2(\delta_0)_{-45}\right) = I(2\omega_0)_{cal(-45)} \quad \ldots(3.10b)$$

Again, these calibration values are found for both orientations with the analyzer fixed. A more detailed analysis of the derivation of these equations can be found in appendix A.

Experimental Process

The collection of data and calculation of ellipticity is completely automated. Each data point corresponds to calculation of the real part of ellipticity and imaginary part of ellipticity (the coefficient of ellipticity, $\overline{\rho}$). Using the signal from the modulator control as reference, the lock-in measures the ω_0 (50 kHz) component of the intensity. Using the phase value found during calibration, the lock-in phase shifts the reference signal to match the phase of the measured signal, multiplies the two signals together, and finds the mean of the resulting AC signal. Taking the ratio of this signal and twice the calibration maximum results in the imaginary part of the ellipticity

$$\frac{I(\omega_0)_{signal(+45)}}{2I(\omega_0)_{calibration(+45)}} = \frac{\pm -2aJ_1(\delta_0)_{+45}\sin\Delta_{+45}}{\pm -4J_1(\delta_0)_{+45}} = \frac{a_{+45}(\sin\Delta_{+45})}{2}$$

$$= \frac{2\rho_{+45}\sin\Delta_{+45}}{2\left(1+\rho_{+45}{}^2\right)} = \rho_{+45}\sin\Delta_{+45} = \mathrm{Im}(\rho_{+45}) \quad \ldots(3.11a)$$

where the component signals and Δ are defined as above. Close to the Brewster angle, r_p is very small, thus $\rho = r_p/r_s$ is very small and $\left(1+\rho^2\right)$ is very close to 1 (with an ellipticity of 0.03, the resulting error is 0.1%). The second PMT measures the signal at the other orientation (-45) and calculates its ellipticity the same way. There is no rotation of the analyzer during this process – the measurements taken at each exit represent the measurements at each orientation. These two values are then averaged to find the final coefficient of ellipticity.

$$\frac{I(\omega_0)_{signal(-45)}}{2I(\omega_0)_{calibration(-45)}} = \frac{\pm -2aJ_1(\delta_0)_{-45}\sin\Delta_{-45}}{\pm -4J_1(\delta_0)_{-45}} = \frac{a_{-45}(\sin\Delta_{-45})}{2}$$

$$= \frac{2\rho_{-45}\sin\Delta_{-45}}{2\left(1+\rho_{-45}{}^2\right)} = \rho_{-45}\sin\Delta_{-45} = \mathrm{Im}(\rho_{-45}) \quad \ldots(3.11b)$$

$$\overline{\rho} = \mathrm{Im}(\rho) = \left[\mathrm{Im}(\rho_{+45}) - \mathrm{Im}(\rho_{-45})\right]/2 \quad \ldots(3.12)$$

The negative is needed in the average, as the signals at each orientation will always have opposite signs. The lock-ins are then reset and told to record the $2\omega_0$ (100 kHz) component of the signal, which results in the real part of the ellipticity.

$$\frac{I(2\omega_0)_{signal(+45)}}{2I(2\omega_0)_{calibration(+45)}} = \frac{\pm 2aJ_2(\delta_0)_{+45}\cos\Delta_{+45}}{\pm 4J_2(\delta_0)_{+45}} = \frac{a_{+45}(\cos\Delta_{+45})}{2}$$

$$= \frac{2\rho_{+45}\cos\Delta_{+45}}{2\left(1+\rho_{+45}{}^2\right)} = \rho_{+45}\cos\Delta_{+45} = \mathrm{Re}(\rho_{+45}) \quad \ldots(3.13a)$$

$$\frac{I(2\omega_0)_{signal(-45)}}{2I(2\omega_0)_{calibration(-45)}} = \frac{\pm 2aJ_2(\delta_0)_{-45}\cos\Delta_{-45}}{\pm 4J_2(\delta_0)_{-45}} = \frac{a_{-45}(\cos\Delta_{-45})}{2}$$

$$= \frac{2\rho_{-45}\cos\Delta_{-45}}{2\left(1+\rho_{-45}{}^2\right)} = \rho_{-45}\cos\Delta_{-45} = \mathrm{Re}(\rho_{-45}) \quad \ldots(3.13b)$$

$$\mathrm{Re}(\rho) = \left[\mathrm{Re}(\rho_{+45}) - \mathrm{Re}(\rho_{-45})\right]/2 \quad \ldots(3.14)$$

All of these observations and calculations result in one set of data points. The process repeats over a time period specified by the experimenter.

Testing

After each calibration, the ellipsometer was tested on a control surface to make sure it was functioning correctly. The surface used is a 100nm oxide coated silicon wafer, originally used by Jae-Hie Cho in previous experiments with the liquid surfaces group. The wafer was tested on a top-incident vertical ellipsometer in the fall of 2006 by finding the real and imaginary parts of rho as a function of the incident angle of the laser light. Measurements over the span of 30 degrees (from the vertical) to 80 degrees had shown a high level of repeatability, with a variance of no more than 5 percent at the widest angle.

This data was used as the control data during the initial tests of the inverted ellipsometer, and as a test following each calibration. To run the experiments, the prism is removed from the sample holder, and the wafer inverted and placed on the holder such that the light is incident on the testing side. After leveling the wafer, the ellipsometer's arms are moved such that the laser is incident at 80 degrees from the normal on the wafer. The experiment is run and three data points are collected (to make sure there is no time dependence on the measurement, as there should be none during these tests). The incident angle is adjusted five degrees to a 75 degree incidence, and the test repeated. This continues until the measurement at 45 degree incidence – limitations in the design prevent the arms from moving further without damage.

Comparison of the test data – including the initial 2006 tests mentioned above, and tests conducted on the inverted ellipsometer in late 2006 and early 2007 show agreement within the data, within five percent at a 45 degree incidence.

Figure 3.4 Comparison of 2006 Si Wafer Data and Inverted Ellipsometer Wafer Test Data

	RP/RS					
Angle	CodiIm	CodiRe	DanAugIm	DanAugRe	DanAprIm	DanAprRe
80	-0.331858	-0.407360	-0.291814	-0.386545	-0.307683	-0.364585
75	-0.438778	-0.262690	-0.407264	-0.259772	-0.422756	-0.247509
70	-0.483666	-0.108249	-0.464897	-0.106164	-0.478001	-0.088230
65	-0.481608	0.045685	-0.475848	0.049653	-0.490303	0.053073
60	-0.445137	0.171447	-0.450114	0.184202	-0.457734	0.192908
55	-0.386284	0.272970	-0.396092	0.295834	-0.398615	0.303562
50	-0.321883	0.343909	-0.331421	0.377518	-0.331699	0.385318
45	-0.242830	0.394416	-0.263938	0.433403	-0.251471	0.412800
40	-0.183978	0.416224				
35	-0.132668	0.412830				

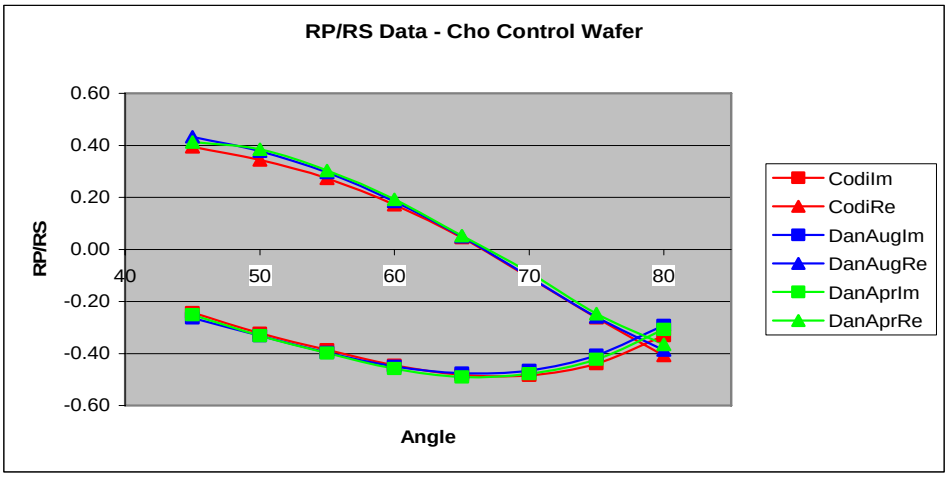

'Codi' – 2006 Wafer Data; 'DanAug' – Fall 2006 Wafer Test Data; 'DanApr' – Spring 2007 Wafer Test Data

Taq Polymer Adsorption and Contact Angle Measurement

The initial experimental work on the Taq Enzyme was conducted with the camera/microscope system and FTA32 software alone. The ellipsometer, while finished, had yet to produce the correct test data at this time. The goal of these first experiments was the verification of the Univ. of Calgary's observations. The light source (Cole-Parmer 41723 150W) is placed behind a lab jack, on which lens tissue and a substrate coated slide is placed. A small needle head is held over the surface where the drop will be applied, and the slide location and camera focus is adjusted until the head is seen clearly. The substrates used were glass slides spin coated with the SU-8 photoresist in Canada, and shipped with the Enzyme samples.

The FTA32 software is set to capture video at one frame per second, which was found to be short enough to observe adsorption over the ten minute time frame. FTA32's recording is started, and the drop is applied to the substrate. There was problems applying the same volume of sample over different runs, but this proved to be somewhat of an advantage, as the effect of volume on adsorption can be observed. Any small changes in focus are completed quickly, and the drop is left for at least ten minutes, or until any observed contact angle changes end after that period. Once the experiment is complete, the FTA software is used to analyze each frame. By manual application of the surface line and a line of curvature, the program calculates contact angle, drop base width, volume, and other parameters.

Another goal of the work was to attempt to find an alternate substrate that resulted in the adsorption and contact angle change observed on the SU-8. These silane substrates were applied using vapor deposition. A clean glass microscope slide is cut into approximately a one inch square. The square is sonicated in acetone, ethyl alcohol, and toluene for five minutes each, and blown dry using nitrogen gas after each step. A snow jet is applied to the slide (carbon dioxide applied at high pressure onto the heated slide), and plasma cleaned for five minutes. The slides are then placed in a deposition chamber (Petri dish), which has been surrounded with phosphorus pentoxide and left to dry out for ten minutes due to the violent reaction between the silanes and water. The entire setup is enclosed in a larger closed dish. A small drop (approx. 0.15mL) of the silane is added elsewhere in the chamber, and left to set in the closed chamber for ten minutes. The slide is removed, and the contact angle is tested as above.

Figure 3.5 Example of a FTA32 Contact Angle Analysis

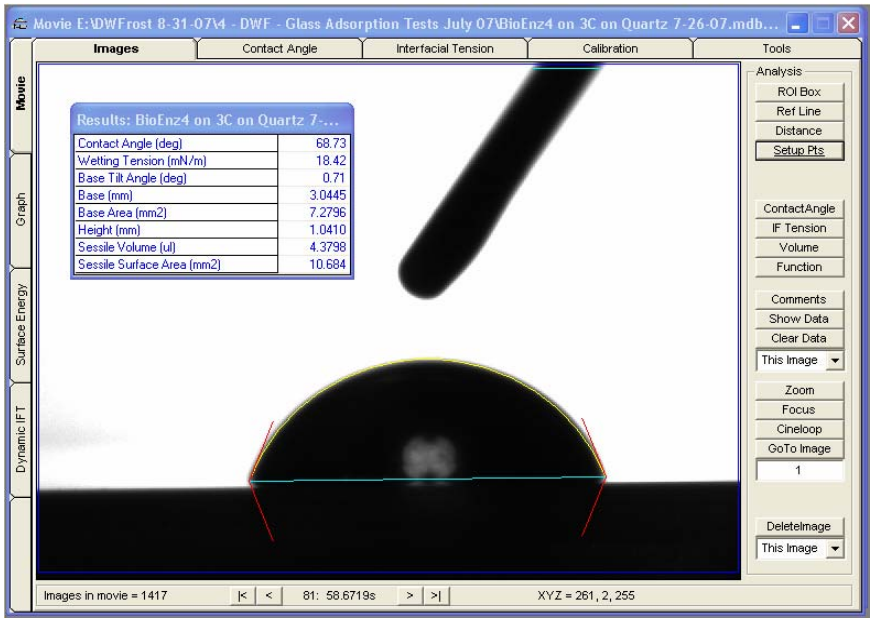

Gold Nanoparticle Adsorption and the Ellipsometer

With the completion and testing of the ellipsometer, work began on nanoparticle adsorption, which was observed at the glass-nanoparticle solution interface using ellipsometry. A sample chamber was constructed by securing a 0.3 inch long piece of glass tubing (inside diameter 0.86 inches) onto a glass microscope slide with UV set glue, which was found to be resistant to the standard cleaning procedure (sonication in acetone, ethyl alcohol, and toluene) when applied correctly. The ellipsometry experiment itself is primarily computer controlled. The lock-in settings and data acquisition are performed by a program written by Matthew Brown and Codi Gharagouzloo and modified by the author, via a National Instruments PCI-GPIB internal computer control card and NI-488.2 software.

Using the NI software, the arms are user set so that the laser light is incident at 45 degrees to the surface, so that it is perpendicular to the entrance face of the prism. The Brewster angle for this interface (glass-toluene) is slightly more, at 45.75 degrees. 45 degree incidence was chosen because of the simplicity of the construction, as right prisms are readily available. Because the real part of the ellipticity is not zero at this angle, both the real and imaginary parts of the ellipticity were observed during the experiment. A layer of index matching fluid is applied to the prism, and the sample chamber carefully placed on to remove any air between them.

Upon execution of the program, the user must manually input all of the calibration values found using the process outlined above and the time which the program should run. The program sends these values, along with the proper filter and sensitivity settings to the lock-ins. One mL of toluene is then added to the sample chamber, and covered with a glass slide for 20 minutes. This allows the toluene to evaporate into the chamber, so evaporation effects which could cause a change in concentration are minimized during the experiment. After 20 minutes, the program is allowed to begin collecting data. This glass-toluene baseline provides a comparison to the nanoparticle solution later, and also serves as a check on the equipment. After 5 minutes, enough of the nanoparticle solution is added to the toluene to result in the desired concentration. Each experimental run was allowed to collect for at least one-half hour, long enough for the resulting ellipticity reading to stabilize (see chapter 4). At completion, the resulting diluted solution was collected for further analysis by the liquid surface group.

CHAPTER 4 - Results and Analysis

Taq Enzyme Adsorption

The Taq contact angle measurements were ran using the camera/microscope system as outlined above, in an open air environment. At the time it was unknown how much effect, if any, evaporation would have on our data. The first run consisted of a 3.65 µL drop of enzyme solution on a pre-spun coat of SU-8 photoresist on glass. After about four minutes, there was an obvious reduction in droplet size. After five minutes, the drop had reduced enough to affect the accuracy of the FTA32 software, as the evaporation off the top of the drop had misshapened the drop, making contact angle analysis unreliable.

Figure 4.1 First Drop of Taq Enzyme on SU-8 Over A Five Minute Period

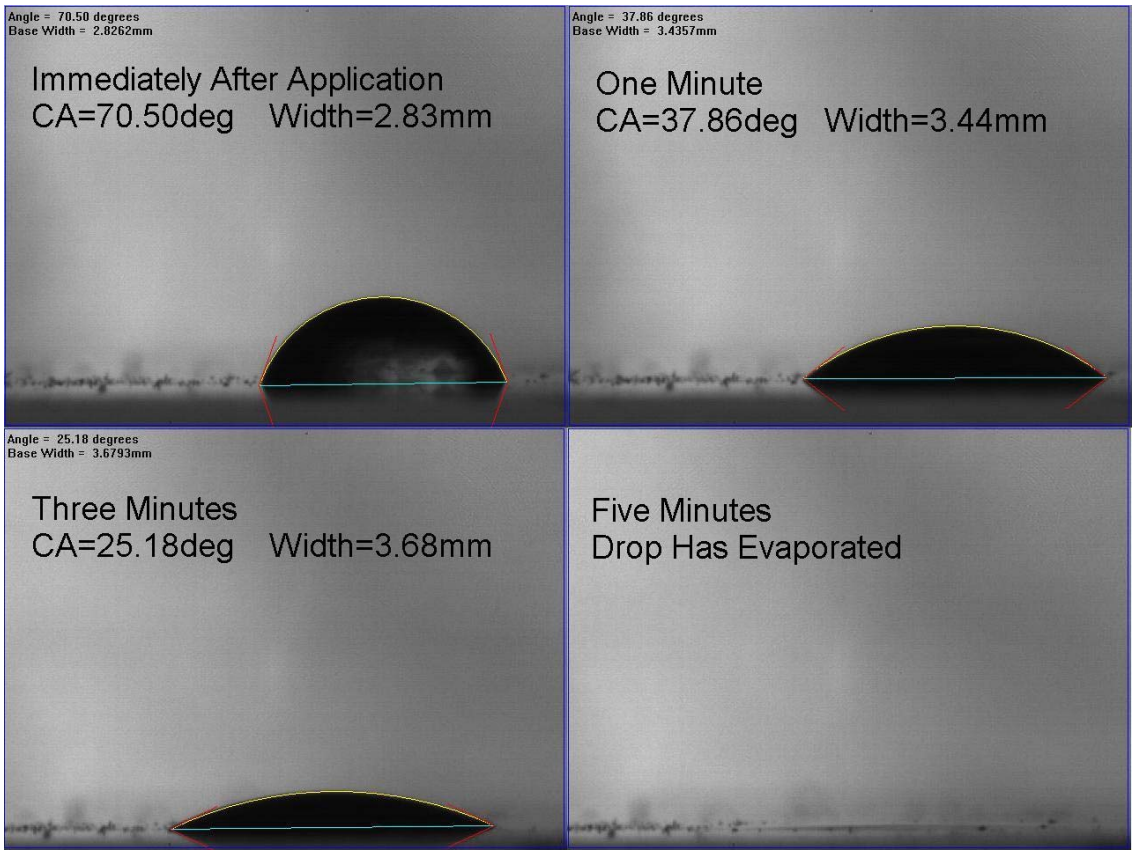

The result was a definite contact angle change over the observation period, but it is difficult to tell how much is caused by evaporation of the solution. The plot of contact angle and volume versus time indicates that evaporation begins immediately, but contact angle falls much sharper in the first two minutes of the experiment than in the remainder.

Figure 4.2 Contact Angle and Volume vs. Time for the First Enzyme Drop on SU-8

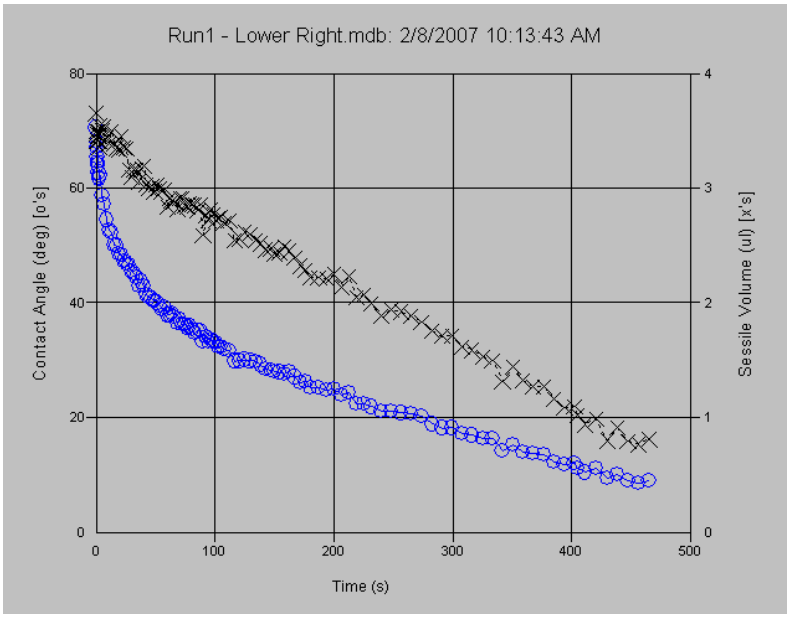

Figure 4.3 Contact Angle and Base Width vs. Time for the First Enzyme Drop on SU-8

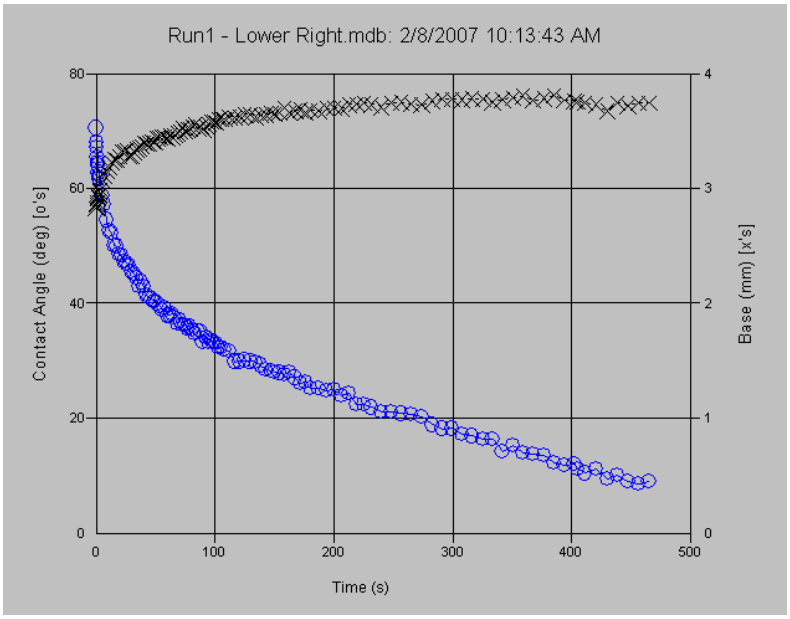

Contact Angle in Blue, Base Width in Black

It was observed that in this first two minutes, the base of the drop spread out rapidly and then slowed in the later minutes. The base area of the drop is an indicator of surface energy, thus it appears that there is contact angle change due to adsorption in the first two minutes, after which the change is driven by evaporation. This can be seen easier if base width is plotted instead of volume (Figure 4.3). After four minutes, the base ceases to spread out while the contact angle continues to drop due to evaporation off the top of the droplet. Over the entire run, contact angle changed from 70 degrees to 10 degrees. A second, larger drop (5.8 µL) was observed elsewhere on the same slide with similar results.

Figure 4.4 Contact Angle and Base Width vs. Time for the Second Enzyme Drop on SU-8

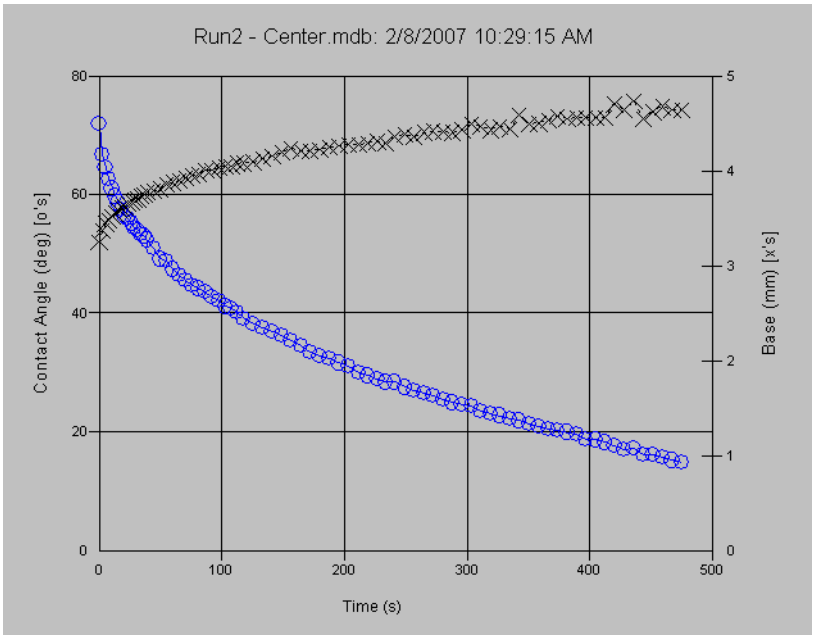

Like the first drop, there is a steep contact angle change in the first two minutes as the drop's base increases in size. The base then begins to stabilize, though the base is still growing at the four minute mark, at which point the first drop had stopped spreading. Like the first run, there is an overall contact angle change of about 60 degrees, but much of it can be attributed to other factors. As previously stated, CA change is driven primarily by evaporation after two to three minutes. Because data is taken immediately after the drop is applied, gravity may be affecting spread in the first seconds. Of note in this data is the fact, while there was some contact angle change due to adsorption, it was not as much as that observed at the University of Calgary. It also appears that the adsorption in our experiments occurs quicker than the ten minutes observed by UC.

Also of importance was finding a substitute for the SU-8 substrate that could be applied as a smoother layer, but retains the properties of SU-8, a high initial contact angle (80 to 90 degrees) and a high contact angle change (strong adsorption). Our group found that silanes could be applied readily using the vapor deposition procedure, and produce similar results to the SU-8. The Adsorption of the Taq Enzyme was tested on two of these silanes.

An 18.38 µL drop of the Enzyme was applied to a slide vapor deposited with (3-cyano-propyl)tricholorsilane (Acros Organics 99%) over a period of ten minutes.

Figure 4.5 Contact Angle and Base Width vs. Time for the Enzyme Drop on 3-Cyano

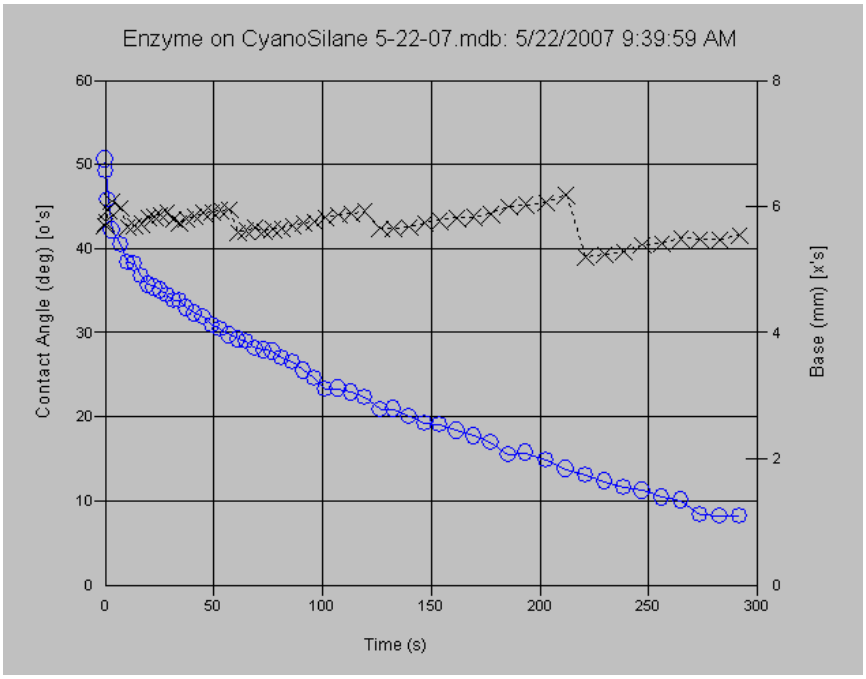

Due to a small error in camera placement, the sample-camera distance had to be occasionally adjusted to fit the entire drop in the image so contact angle could be measured accurately. Because the FTA32 calculates base width based on the initial camera placement, this adjustment resulted in the jumps seen in the base width data. The actual measurement of base width is inaccurate in this graph after the first jump. The contact angle was much smaller initially, 50 degrees as opposed to 70 degrees, but it is noted that the base continues to increase through the whole experiment, until the contact angle becomes too small to provide accurate data. More of the contact angle change in this case is due to adsorption, though an ideal replacement would have a higher initial contact angle.

The enzyme was also tested on 1,1,2,2-Perfluorodecyldymethylchlorosilane (Alfa Aesar) in the same manor.

Figure 4.6 Contact Angle and Base Width vs. Time for the Enzyme Drop on MonoFChloro

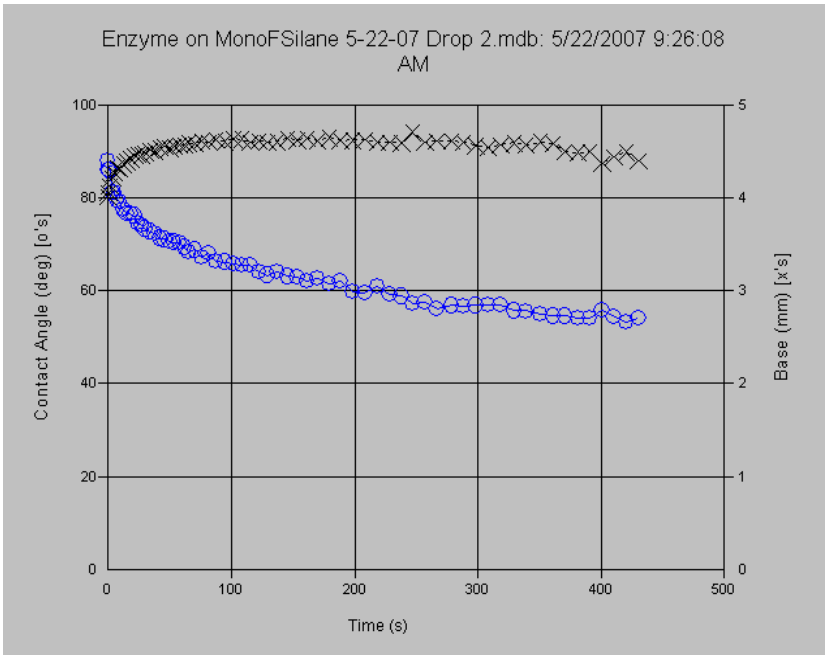

Again, this results in one of our requirements being met, but not the other. The initial contact angle (nearly 90 degrees) is higher than that observed on the SU-8, but there is much less contact angle change, less than 40 degrees over the span of the experiment.

Figure 4.7 Contact Angle and Base Width vs. Time for the Enzyme Drop on Teflon

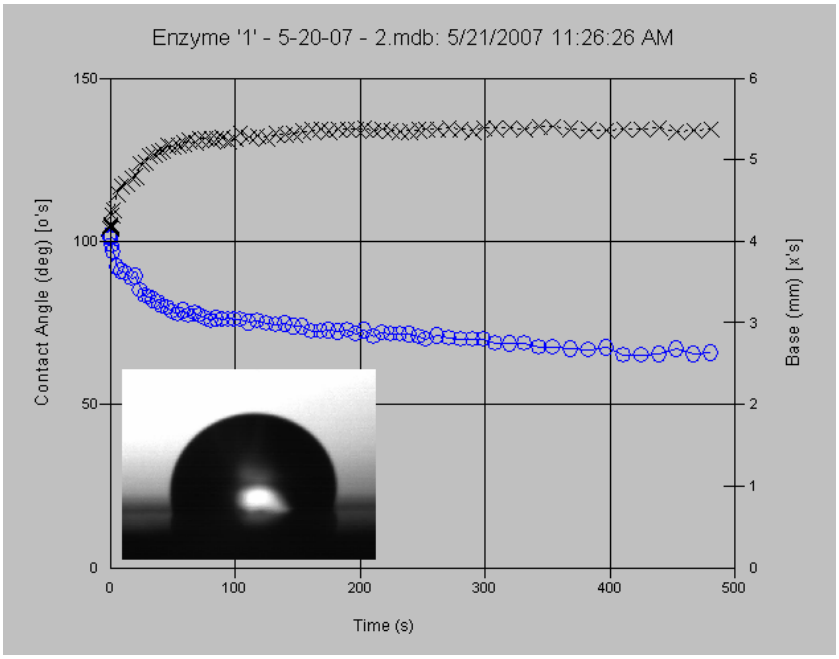

The enzyme was also tested on a sheet of Teflon, a material known to be highly hydrophobic. The white pre-fabricated sheet would not be ideal for the inverted ellipsometry setup, but the contact angle was observed to determine whether it could be useful in other experiments. The initial contact angle was adequate at 102 degrees (insert in Figure 4.7), but again, the contact angle change was smaller than that of the SU-8 at about 40 degrees. The process also happens quickly, as the drop ceases spreading after less than two minutes.

The enzyme was also tested on bare glass, silicon, and quartz, to see if there were any adsorption effects on the uncoated surfaces alone. In all of these cases, the initial contact angle was less than twenty degrees, and very little to no contact angle change was observed. In this research, the substrates were the driving force behind the observed adsorption.

Gold Nanoparticle Adsorption

The experimental ellipsometry work focused on adsorption of a diluted gold nanoparticle solution at the glass-solution interface. The initial experiment consisted of the addition of dodecanethiol (DT), to the toluene in various concentrations. These tests were conducted to see if dodecanethiol, used in the fabrication of the gold nanoparticles, alone shows adsorption effects. The experiment began with the addition of 0.68 mL of toluene, and observation of the glass-toluene baseline. Dodecanethiol was added every fifteen minutes.

Figure 4.8 Ellipticity of Various Concentrations of Dodecanethiol in Toluene

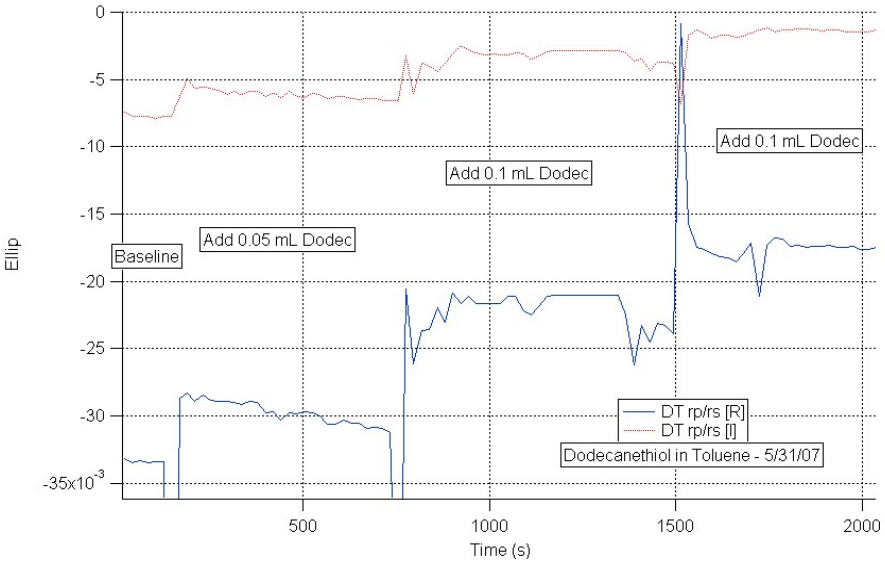

The spikes between additions are likely due to bulk movements throughout the sample as an additional amount of DT is being added. The initial addition of a smaller amount of DT resulted in a decrease of ellipticity of about 20 percent; subsequent additions resulted in little change over time. The first NP experiment started with 0.70 mL of toluene to establish the baseline, and the addition of 0.05 mL of the NP solution (6.7% solution), and the later addition of 0.1 mL of NP (17.6% solution).

<u>Figure 4.9</u> Ellipticity of Gold NP in Toluene – First Experiment

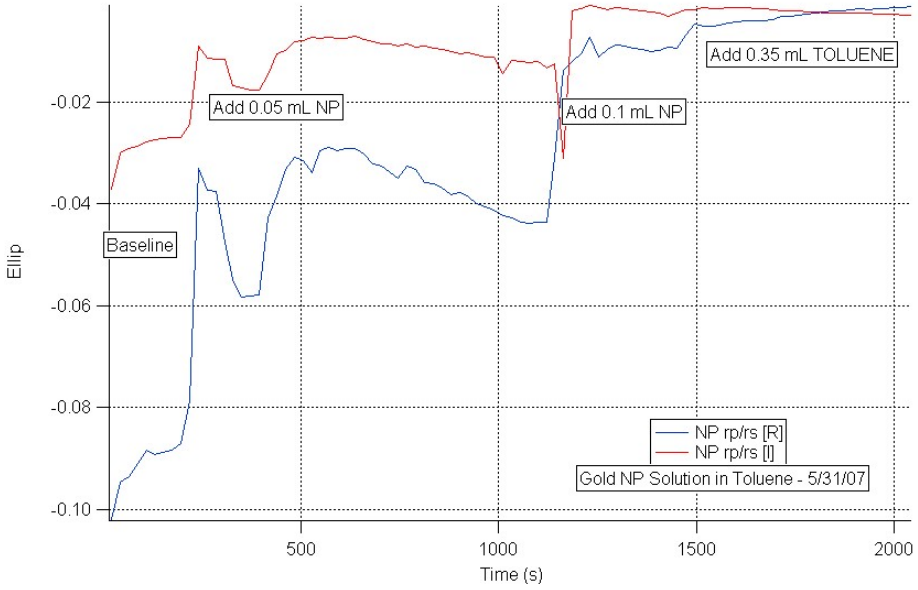

Addition of the gold NP resulted in a sharp initial rise and fall about one minute later. The ellipticity rises again to near its original peak, and begins to fall and level out. The second addition caused another jump and smaller fall, without the 'trench' present after the first addition. It was initially estimated that the initial rise and falls may be due to bulk movements throughout the sample, as opposed to on the interface.

The following experiment consisted of addition of NP solution every ten minutes. The baseline consisted of 1 mL of toluene observed for 5 minutes, and 0.1 mL of NP solution added every ten minutes after for resulting concentrations of 9.1%, 16.7%, 23.1%, 28.6%, and 33.3%. The ellipsometer was recalibrated before this experiment, and the resulting analyzer position and means by which the average signal between the two orientations is calculated, results in the positive data for Re(ρ), as opposed to the negative data in previous experiments.

<u>Figure 4.10</u> Ellipticity of Various Concentrations of Gold NP in Toluene – Second Exp.

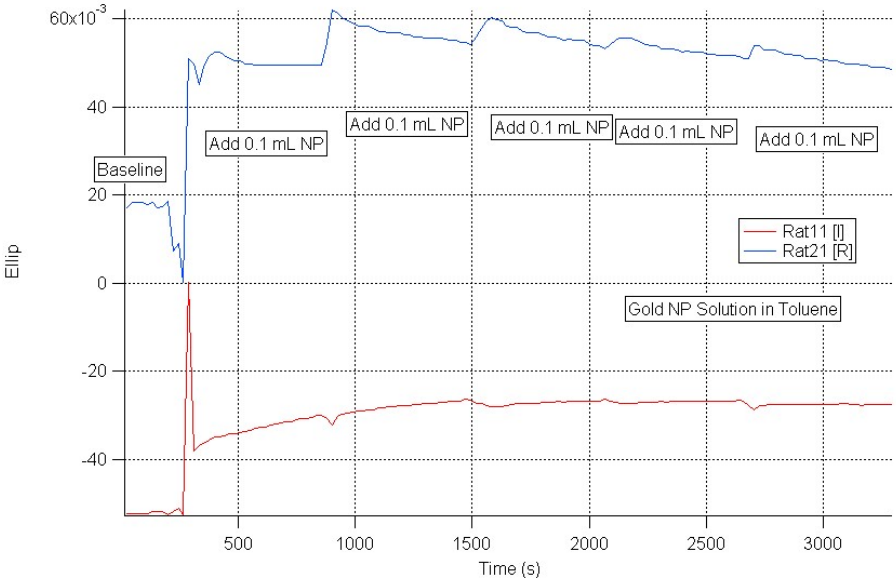

With the first addition, the jump and dip seen with the first experiment is also seen. Subsequent additions also demonstrate this dip and rise pattern, but on a smaller scale. The experimental data, overall, stabilizes independent of the concentration. This may also be an effect of bulk movement of the solution. Until this point, the resulting NP-toluene solution data had not been allowed to stabilize after a single add. A very small amount (0.005mL) of the gold NP was added to 1 mL of toluene, and observed for 40 minutes.

<u>Figure 4.11</u> Ellipticity of a 0.5% Gold NP Solution over 40 Minutes

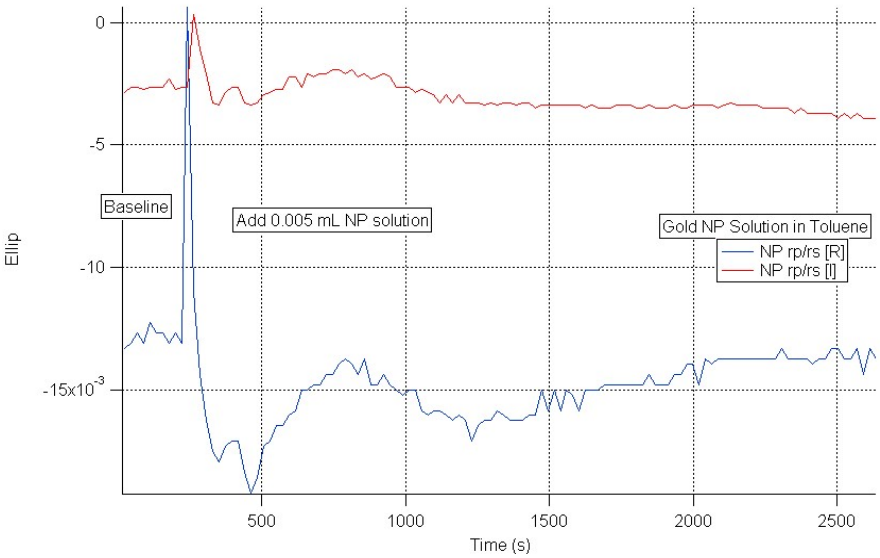

The same time dependent pattern is seen as in the previous experiments, and the solution's ellipticity appears to start stabilizing after 20 minutes. The resulting change in ellipticity is 10 to 15 percent. To see whether there was a concentration dependence on the resulting ellipticity, 0.55 mL of the pure NP solution was observed over 30 minutes. In this case, the established baseline was the glass-air interface as opposed to the glass-toluene baseline.

<u>Figure 4.12</u> Ellipticity of the Pure NP Solution over 30 Minutes

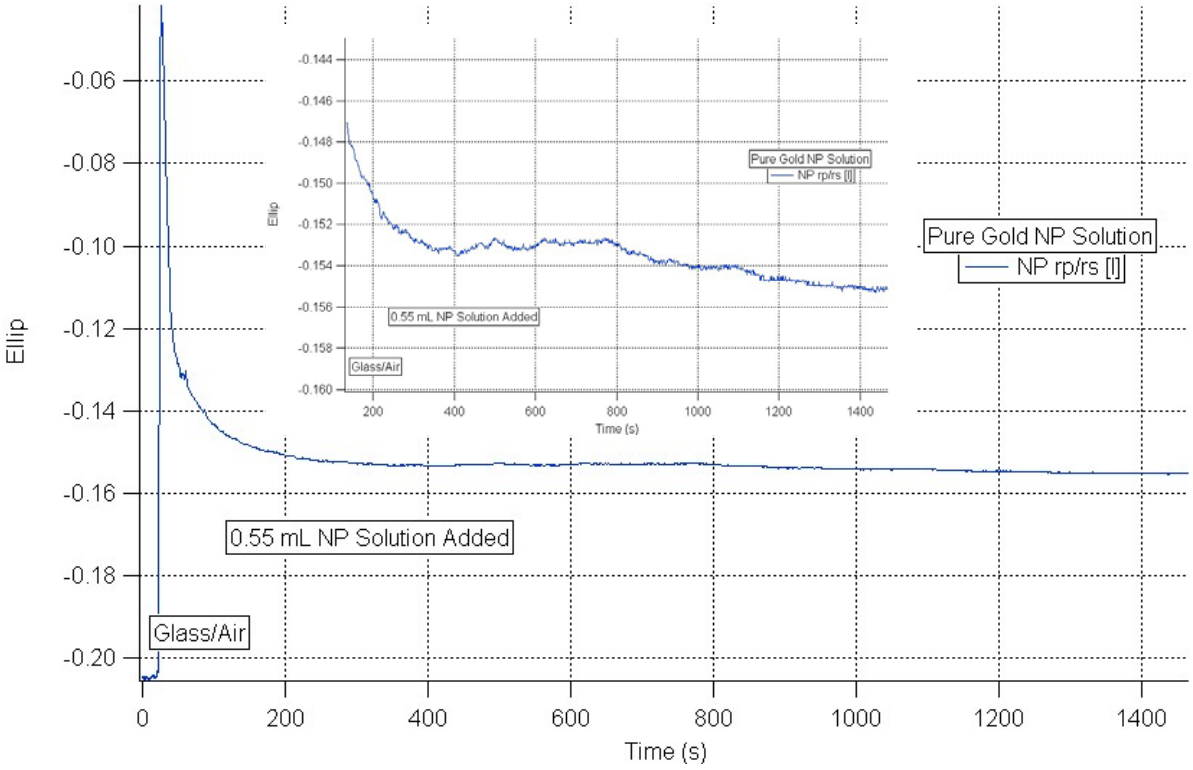

The resulting change in ellipticity is large (from the Toluene baseline of about 0.013 to 0.155), and while it is harder to see, the 'bump' in the data still exists (insert of Figure 4.12). A final experiment was conducted to investigate another concentration and to illustrate consistency in the data. 0.02 mL of gold NP was added to 1.5 mL of toluene, creating a 1.3% solution. The experiment was run as done previously. Again, like the other experiments, a 'bump' is still present in the data, but the ellipticity begins to increase after 30 minutes. By this point, however, the sample of nanoparticles used in all of these experiments may have become contaminated due to exposure to the air.

<u>Figure 4.13</u> Ellipticity of a 1.3% Gold NP Solution over 30 Minutes

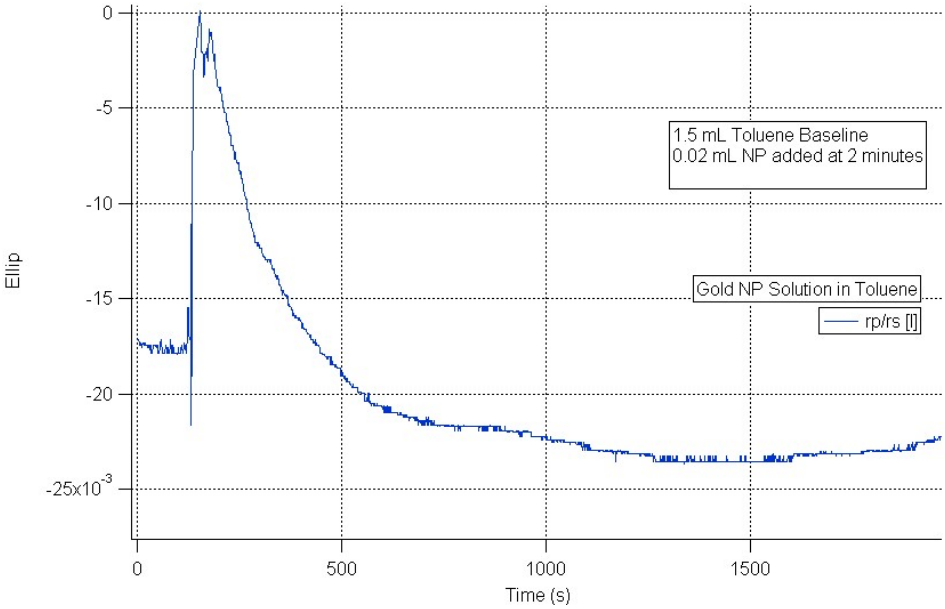

After discussion with Dr. Bruce Law, it was agreed that the bump pattern observed in all of the data is likely due to bulk changes over the whole sample as opposed to changes at the interface itself. This could be caused by laser reflection from both the interface and off of the particles themselves entering the analyzer, so that movements in the solution register as ellipticity changes. It is believed that by using a small drop, similar to that of the enzyme experiments, the effects of the bulk changes will be reduced. Investigation of this phenomenon will continue by the liquid surfaces group, including tests on other substrates.

CHAPTER 5 - Discussion and Experimental Extensions

In this experiment, it was shown that the constructed ellipsometer works as a way to observe ellipticity and thus properties of a liquid-solid interface over time. Integration with the camera/microscope system, which the design of the ellipsometer will easily allow, will result in simultaneous ellipticity and contact angle measurements, providing more information about what is occurring at the interface.

With the contact angle measurement system, the observations of A.R. Prakash at Calgary were verified to an extent, though extended cold storage (our samples were kept in the freezer for at least six months before observations began) may have affected our results. Included in the liquid surface group's future work will be observation of fresh samples to verify this.

An important measure to consider is the fact that observations including a substrate coating do not purely consist of the solid-liquid boundary and intermediate layer. The substrate layer must also be considered in the calculations. Frank Male of the Law surfaces group has been working on theoretical data to find the effect of a thickness of the SU-8 on the resulting ellipsometry measurements.

The initial observations reported here are just the beginnings of a number of experiments possible with this equipment. As mentioned above, integration of the contact angle and ellipsometry systems, along with immersing the sample in oil during observation to prevent the observed evaporation effects, will give a clearer picture of the adsorption occurring at the interface. The sample holder design allows for easy switching of substrates, providing a means to investigate many different substrates. Likewise for the gold nanoparticles and any other solution under investigation, as the setup is the same for any material under investigation. The observation of the gold nanoparticles in this situation is imperative, as the bulk shifts observed in the data for the large sample amount may be reduced if a small drop is used, such as those used in the taq enzyme work.

Other extensions to this work include spectroscopic ellipsometry, where the polarization of reflected light is observed over a number of incident wavelengths. The resulting ellipsometry vs. wavelength data is of great interest to us. We may also 'take a look' at the adsorption layer

using Brewster angle microscopy. Instead of the photomultiplier and intensity measurement system, a camera records the reflected light as the incident position of the layer is changed.

Figure 5.1 Overview of Brewster Angle Microscopy System

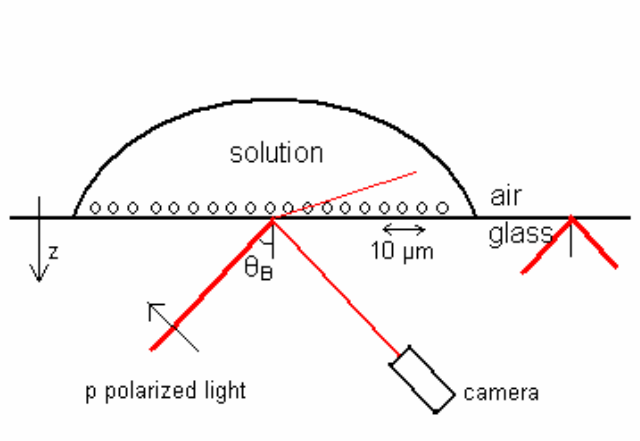

In this process, P polarized light is sent to the interface at the Brewster angle defined by the solid-solvent interface. If not focused on the drop, all of the resulting light will be reflected to the camera (as the Brewster angle will be greater than the critical angle for the air-glass interface). If nothing exists at the interface (no thin film), none of the polarized light is reflected to the camera. The presence of a film affects the Brewster angle value, and as a result some of the light is reflected to the camera. Moving the point of incidence around results in an 'image' of the adsorption layer; the system will have a spatial resolution of about 10 micrometers.

References

Auroux, P.A., Koc, Y., deMello, A., Manz, A., and Day, P.J.R., 2004, Miniaturized nucleic acid analysis, *Lab on a Chip*, http://www.rsc.org/ej/LC/2004/b408850f/ (September 7, 2007).

Beaglehole, D., 1980, Ellipsometric Study of the Surface of Simple Liquids, *Physica* 100B:163-174.

Chollet, F., Editor, 2007, SU-8: Thick Photo-Resist for MEMS, http://memscyclopedia.org/su8.html (September 7, 2007).

Hecht, E., 2002, *Optics*, 4th ed., Addison Wesley, San Francisco, 698 p.

Law, B.M., 1984, Properties of Interfaces, Doctoral Thesis, Victoria University of Wellington.

Lorentz, H., Despont, M., Fahrni, N., LaBianca, N., Renaud, P., and Vettiger, P., 1997, SU-8: A Low-Cost Negative Resist for MEMS, *J. Micromech. Microeng.* 7:121-124.

Marris, E., 2006, 2006 Gallery: Brilliant Display, *Nature* 444:985-991.

Prakash, A.R., Pilarski, L.M., Backhouse, C.J., and Kaler, K.V.I.S., 2005, A Functionally Integrated Microfluidic Device for Genetic Analysis, Proc. *Of ISSS2005 International Conference on Smart Materials, Structures, and Systems*.

Prasad, B.L.V., Stoeva, S.I., Sorensen, C.M., and Klabunde, K.J., 2002, Digestive Ripening of Thiolated Gold Nanoparticles: The Effect of Alkyl Chain Length, *Langmuir* 18:7515-7520.

Appendix A - Propagation of Laser Light Through the Ellipsometer

Following the optical component alignment procedure, light exiting the polarizer is polarized at 45º relative to the s and p directions, thus the s and p components both have 1/√2 strength of the laser signal.

$$\tilde{E} = E_0\left(\frac{\hat{\tilde{s}}}{\sqrt{2}} + \frac{\hat{\tilde{p}}}{\sqrt{2}}\right) \quad \ldots(A.1)$$

Passing through the birefringence modulator (which is aligned with the s and p directions) imparts a phase shift δ on the p polarized light.

$$\tilde{E} = \frac{E_0}{\sqrt{2}}\left(\hat{\tilde{s}} + e^{i\delta}\,\hat{\tilde{p}}\right) \quad \ldots(A.2)$$

Reflection off of the interface results in both an amplitude change and phase shift in both s and p polarizations, depending on the properties of the interface.

In general: $E_r = |r|e^{i\delta}E_0$ (A.3), thus

$$\tilde{E} = \frac{E_0}{\sqrt{2}}\left(|r_s|e^{i\delta_s}\hat{\tilde{s}} + |r_p|e^{i(\delta_p+\delta)}\hat{\tilde{p}}\right) \quad \ldots(A.4)$$

The resulting signal is analyzed at ± 45º to the s and p orientations – both directions are measured to account for any minor systematic inconsistencies in the device.

$$\left|\tilde{E}_{\pm 45}\right| = \left|\frac{1}{\sqrt{2}}\tilde{E}_s \pm \frac{1}{\sqrt{2}}\tilde{E}_p\right| = \left|\frac{1}{\sqrt{2}}\left(\tilde{E}_s \pm \tilde{E}_p\right)\right| = \left|\frac{E_0}{2}\left(|r_s|e^{i\delta_s}\hat{\tilde{s}} \pm |r_p|e^{i(\delta_p+\delta)}\hat{\tilde{p}}\right)\right|$$

...(A.5)

The measured intensity is this field squared.

$$I = \left|\tilde{E}\right|^2 = \left(\frac{E_0}{2}\right)^2\left(|r_s|e^{i\delta_s}\hat{\tilde{s}} \pm |r_p|e^{i(\delta_p+\delta)}\hat{\tilde{p}}\right)^2 \quad \ldots(A.6)$$

Squaring the latter term of the intensity (using complex rules):

$$\left(\left|r_s\right|e^{i\delta_s}\hat{\tilde{s}} \pm \left|r_p\right|e^{i(\delta_p+\delta)}\hat{\tilde{p}}\right)^2 = \left(\left|r_s\right|e^{i\delta_s}\hat{\tilde{s}} \pm \left|r_p\right|e^{i(\delta_p+\delta)}\hat{\tilde{p}}\right)\left(\left|r_s\right|e^{-i\delta_s}\hat{\tilde{s}} \pm \left|r_p\right|e^{-i(\delta_p+\delta)}\hat{\tilde{p}}\right) =$$
$$r_s{}^2 + r_p{}^2 \pm \left(r_s r_p e^{i(\delta_p+\delta-\delta_s)} + r_s r_p e^{-i(\delta_p+\delta-\delta_s)}\right) =$$
$$r_s{}^2 + r_p{}^2 \pm r_s r_p \left(e^{i(\delta_p+\delta-\delta_s)} + e^{-i(\delta_p+\delta-\delta_s)}\right) =$$
$$r_s{}^2 + r_p{}^2 \left(1 \pm \frac{r_s r_p}{r_s{}^2 + r_p{}^2}\left(2\cos\left[\delta_p - \delta_s + \delta\right]\right)\right)$$

…(A.7)

The definition of cosine is used to simplify the exponentials.

By defining the difference in the p and s phase shifts as $\Delta = \delta_p - \delta_s$

and the term a as $a = \frac{2r_s r_p}{r_s{}^2 + r_p{}^2} = \frac{2r_s{}^2\left(r_p / r_s\right)}{r_s{}^2\left(1 + \left(r_p{}^2 / r_s{}^2\right)\right)} = \frac{2\rho}{1+\rho^2}, \rho = \frac{r_p}{r_s}$

and $I_0 = E_0{}^2$, the resulting intensity is:

$$I = \frac{I_0}{4}\left(r_s{}^2 + r_p{}^2\right)\left(1 \pm a\cos(\Delta + \delta)\right)$$

…(A.8)

The birefringence modulator's phase shift δ has a variation at frequency ω0, such that

$$\sin(\delta) = \sin(\delta_0 \sin\omega_0 t), \cos(\delta) = \cos(\delta_0 \sin\omega_0 t)$$ …(A.9)

Expansion of the cosine term in the intensity results in

$$\cos(\Delta + \delta) =$$
$$\cos\Delta\cos\delta - \sin\Delta\sin\delta =$$
$$\cos\Delta\cos(\delta_0 \sin\omega_0 t) - \sin\Delta\sin(\delta_0 \sin\omega_0 t) =$$
$$\cos\Delta\left[J_0(\delta_0) + 2J_2(\delta_0)\cos^2(\omega_o t) + ...\right] - \sin\Delta\left[2J_1(\delta_0)\sin(\omega_0 t) + 2J_3(\delta_0)\sin^3(\omega_0 t) + ...\right]$$

…(A.10)

where the sinusoidal δ terms have been expanded into their respective Bessel Function series.

Thus, the intensity is (approximating this to the first 3 Bessel Functions)

$$I = \frac{I_0}{4}\left(r_s{}^2 + r_p{}^2\right)\left(1 \pm a\left[\cos\Delta J_0(\delta_0) - \sin\Delta 2J_1(\delta_0)\sin(\omega_0 t) + \cos\Delta 2J_2(\delta_0)\cos^2(\omega_0 t)\right]\right)$$

…(A.11)

First Term

$$I = \frac{I_0}{4}\left(r_s{}^2 + r_p{}^2\right)\left(1 \pm a\left[\cos\Delta J_0(\delta_0)\right]\right) \quad \ldots(A.12)$$

To simplify this DC component of the signal, the positional dependence (between ±45º) needs to be removed. This is done in calibration by removing any interfaces in the system (thus resulting in $\Delta=0$ and $\cos\Delta=1$) and adjusting the voltage applied to the BM until equal intensities are recorded in each orientation. When this is the case, $\delta_0=2.4$ radians, and $J_0(\delta_0)=0$. The DC term then simplifies to

$$I_{DC} = \frac{I_0}{4}\left(r_s{}^2 + r_p{}^2\right) \quad \ldots(A.13)$$

which is kept constant by the current controller feedback system.

Second and Third Terms

If the DC component in the second term:

$$I = \frac{I_0}{4}\left(r_s{}^2 + r_p{}^2\right)\left(1 \pm a\left[-\sin\Delta 2J_1(\delta_0)\sin(\omega_0 t)\right]\right) \quad \ldots(A.14)$$

is kept constant, the AC component is proportional to

$$I_{AC}(\omega_0) \propto \left(\pm -2aJ_1(\delta_0)[\sin\Delta]\right) \quad \ldots(A.15)$$

Likewise, for the third term,

$$I_{AC}(2\omega_0) \propto \left(\pm 2aJ_2(\delta_0)[\cos\Delta]\right) \quad \ldots(A.16)$$

Acquiring Calibration Values

2f phase and $2\omega_0$ voltage

With the instrument straight through, and no interface, there is no difference in the phase shift in the S and P polarizations. Thus, $\Delta=0$, and equations A.15 and A.16 become

$$I_{AC}(\omega_0) \propto 0 \quad \ldots(A.17)$$

$$I_{AC}(2\omega_0) \propto \left(\pm 2J_2(\delta_0)\right) = I(2\omega_0)_{cal} \quad \ldots(A.18)$$

As $\rho = \frac{r_p}{r_s} = 1 \Rightarrow a = \frac{2\rho}{1+\rho^2} = 1$

With the lockin's phase set to minimize the $2\omega_0$ signal, and then phase shifted 90 degrees (to find the maximum signal), the ω_0 signal loses its AC component, while the AC component of the $2\omega_0$ signal is at a max.

f phase and ω_0 voltage

Likewise, when the quarter wave plate is added, with its fast axis in the P orientation, $\Delta=\pi/2$ and $\cos\Delta=0$, thus equations A.15 and A.16 become

$$I_{AC}(\omega_0) \propto (\pm -2J_1(\delta_0)) = I(\omega_0)_{cal} \quad \ldots(A.19)$$

$$I_{AC}(2\omega_0) \propto 0 \quad \ldots(A.20)$$

Measurement

By taking a ratio of the signal measured at this phase (which contains the ellipticity term ρ) and the calibration measurement (which does not contain this term), the ellipticity (and thus the coefficient of ellipticity, the imaginary part of this) can be found.

The $2\omega_0$ signal (whose term contains $\cos\Delta$ corresponds to the real part of the ellipticity and the ω_0 signal (whose term contains $\sin\Delta$) corresponds to the imaginary part.

$$\frac{I(\omega_0)_{signal}}{2I(\omega_0)_{calibration}} = \frac{\pm -2aJ_1(\delta_0)\sin\Delta}{\pm -4J_1(\delta_0)} = \frac{a}{2} = \frac{2\rho\sin\Delta}{2(1+\rho^2)} = \rho\sin\Delta = \mathrm{Im}(\rho) \quad \ldots(A.21)$$

(Close to the Brewster angle, r_p is very small, thus $\rho = r_p/r_s$ is very small and $(1+\rho^2)$ is very close to 1.) The average of these ratios is taken over orientations (+45 and -45) to account for any small systematic errors in the equipment.